Diagnosis of mesenteric ischemia using magnetic resonance spectroscopy

Refocused double-quantum editing for lactate detection in the portal vein

S. Cnossen[1,2,3], R.H. Geelkerken[1,2], C.S. Arteaga de Castro[3], F.F.J. Simonis[4], B. ten Haken[4], G.J. de Borst[5], D.W.J. Klomp[3]

[1] Department of Vascular Surgery, MST, Enschede, The Netherlands

[2] Multi-Modality Imaging (M3i), TechMed Centre, University of Twente, Enschede, The Netherlands

[3] Department of Imaging, University Medical Center Utrecht, The Netherlands

[4] Department of Magnetic Detection and Imaging, University of Twente, Enschede, The Netherlands

[5] Department of Vascular Surgery, University Medical Center Utrecht, The Netherlands

Abstract

Objective

In acute mesenteric ischemia (AMI) the blood flow to the intestine is decreased below the level necessary for the continuous maintenance of aerobic metabolism. Chronic mesenteric ischemia (CMI) occurs when the blood flow to the gastrointestinal (GI) tract gradually decreases to below the level required for all motor, secretory and absorptive activities to function. Nowadays the diagnosis of AMI and CMI is a combination of recognition of the early aspecific clinical symptoms and appropriate assessment of the mesenteric vascular anatomy. To improve the timely diagnosis of AMI and CMI there clearly is a need for a non-invasive, fast and easy applicable test assessing the adequacy of the bowel wall perfusion. The portal vein is the drain of the bowel. Increased lactate concentration indicates anaerobic metabolism.

The aim of the present study is to develop a proton magnetic resonance spectroscopy (1H-MRS) technique which can be used for the measurement of physiological and pathological lactate concentrations in the portal vein for early diagnosis of acute and chronic mesenteric ischemia.

Methods

A 7 Tesla MR system was used to explore the enhanced spectral resolution and increased signal to noise ratio of this field strength for the acquisition of lactate in the portal vein. Spin system simulations were performed to find the best sequence parameters for the best lactate signal detection. Experiments were performed at 7T, where three different 1H-MRS techniques (STEAM, PRESS and DQF) were tested on lactate phantoms (static and with flow up to 924 ml/min) of different concentrations (2.5, 20 and 50 mM lactate). The flow phantom was embedded in either water or oil to test the lipid suppression of each technique. In vivo experiments on the portal vein of two volunteers and the brain of another volunteer were also performed. Additionally, a portal vein simulating MATLAB script was created to calculate the theoretical signal loss caused by the blood flow during the refocused DQF sequence.

Results

Lactate was detected in phantoms containing 2.5, 20 and 50 mM lactate solutions with STEAM, PRESS and the refocused DQF sequence. However, when surrounded by lipids, STEAM and PRESS showed overlapping signals of lactate and lipids on the spectrum. Only

the DQF sequence was able to measure lactate in the presence of lipids. However, part of the signal was lost for all sequences when flow was present. Lactate was detected in the presence of flow (up to 924 ml/min). The in vivo scans did not show a distinguishable lactate peak in the spectrum as it clearly overlapped with the lipids coming from elsewhere and the DQF sequence showed extreme sensitivity to motion due to the strong gradients used. According to the simulations, the signal loss in the lowest portal vein flow was found to be approximately 33% and in the fastest portal vein flow approximately 55%.

Conclusion

The refocused DQF sequence can be used to detect lactate in stagnant phantoms with physiological lactate concentrations in the presence of lipids. However, this sequence is extremely sensitive to motion (i.e. flow, cardiac and breathing motion). The incorporation of velocity sensitive gradients to the refocused DQF sequence is recommended, in addition to flow triggering for an accurate detection of the lactate signal.

Contents

1   Introduction

In acute mesenteric ischemia (AMI) the blood flow to the intestine is decreased below the level necessary for the continuous maintenance of aerobic metabolism [1]. Chronic mesenteric ischemia (CMI) occurs when the blood flow to the gastrointestinal (GI) tract gradually decreases to below the level required for all motor, secretory and absorptive activities to function properly [2, 3].

Most patients with an acute obstruction of the superior mesenteric artery (SMA) experience severe abdominal pain and vomiting [1, 4]. Other symptoms that occur in AMI are indistinct abdominal pain, diffuse tenderness and hypoactive bowel sounds. Classic symptoms observed in CMI are postprandial pain, loss of weight and epigastric bruit. However, this classic triad occurs in a minority of the patients [5-7]. CMI is diagnosed after excluding the more common causes of postprandial abdominal discomfort, weight loss and fatigue.

The challenge for clinicians lies in the early recognition of the clinical picture. One stenotic mesenteric artery may cause longstanding vague abdominal symptoms, while three-vessel stenosis can be accompanied by almost no symptoms [1, 5, 8, 9]. Diagnosing AMI in the early stages is of vital importance as it causes mesenteric infarction and intestinal necrosis if left untreated [10, 11]. The ischemic processes that occur within 6-8 hours after onset are reversible by restoration of blood flow [6].

Imaging techniques as Duplex ultrasound and multislice computed tomography angiography (CTA) are used to assess the mesenteric vascular anatomy [5, 6, 12, 13]. Images of the supplying vessels including collateral arteries created with magnetic resonance angiography (MRA), CTA or digital subtraction angiography (DSA) are sufficient to evaluate for stenosis [14, 15]. However, they cannot be used to diagnose mesenteric ischemia directly [16].

Tonometry and visible light spectroscopy (VLS) are function tests used for diagnosing mesenteric ischemia [1, 5, 17-22]. However, the drawbacks of these tests are that they are invasive and time consuming [18, 23]. Moreover, the balloons used for tonometry will be taken off the market and the negative predictive value of the VLS is low. (Additional information on diagnostic techniques in Appendix A)

Currently, there is a need for a non-invasive, fast and easy applicable

technique that can be used to diagnose acute or chronic mesenteric ischemia in the early stages [24].

The carbon dioxide tension increase observed in ischemia leads to a lactic acid (or lactate) increase as side product. Therefore, lactate concentration is a potential biomarker for diagnosis of mesenteric ischemia. The serological lactate concentration can rise from normal concentrations of 0.5-2.2 mM to 20 mM during ischemia [25]. Measurement of systemic lactate concentrations in peripherally obtained blood samples has been tested to use in diagnosing mesenteric ischemia. However, as other ischemic organs also produce lactate and the liver metabolizes lactate coming from the portal vein fast, systemic lactate elevation is not specific enough to diagnose mesenteric ischemia in an early reversible phase [2, 26].

As all blood from the intestine passes the portal vein before going to the liver, the lactate concentration should be measured in this vein. Portal venous lactate can be measured by obtaining blood samples with a catheter [27]. However, obtaining a blood sample from the portal vein is an invasive procedure.

Lactate can be measured non-invasively with magnetic resonance spectroscopy (MRS), a technique that can measure metabolic information of the tissue by means of a spectrum [28-30]. The signal produced by the hydrogen nuclei (i.e. protons) attached to molecules is observed as a peak resonating at a particular frequency for each different chemical environment the protons encounter in a molecule. The quality of a spectrum is determined by the linewidth and the signal-to-noise ratio (SNR) [28]. Lactate is a J-coupled system with two groups of spins (methine CH2 and methyl CH3) resonating at 4.1 ppm and 1.33 ppm in the proton spectrum. The lactate peak at 1.33 ppm is split into a doublet, because of J-coupling interaction with the methine group [31]. The peak at 4.1 ppm is split into a quartet. Multiple studies have studied lactate concentrations in the body, particularly in cancer applications [32, 33]. J-difference editing methods are known for their measurement efficiency, where two measurements are obtained and subtracted to obtain only the signal of interest (usually the 1.33 ppm doublet that has higher SNR) [34-36]. However, editing techniques require two successive measurements prior subtraction, which makes them prone to motion and flow artifacts (present in the portal vein). The main obstacles that arise when measuring lactate in the portal vein with MRS are the presence of lipids and flow. The methyl

2

group of lactate and the methylene group of the lipids both resonate at a frequency of 1.33 ppm [37, 38]. The spectral overlap of the signals of these groups makes it difficult to differentiate and measure solely lactate.

Stimulated echo acquisition mode (STEAM) and point resolved spectroscopy (PRESS) sequences without editing have been previously tested on phantoms and it was shown that lactate can be detected in the presence of flow [39-44]. Detection of lactate in vivo using STEAM and PRESS has not yet been accomplished.

Multiple quantum filter (MQF) techniques use phase cycling and/or magnetic field gradients to preserve coherence of a particular system of interest, whilst eliminating all others [45]. For example, measuring a lactate signal, whilst suppressing the partially overlapping lipid signal. An MQF transforms a J-coupled system into zero quantum (ZQ) and double quantum (DQ) states. The J-coupled system in DQ state is twice as sensitive to an applied dephasing gradient as a system with or without a different J-coupling [46]. After the system is transformed back to a single-quantum (SQ) state, a rephasing gradient of twice the area of the gradient applied during the DQ state is required for rephasing the signal.

By choosing times between RF pulses and RF center frequencies accordingly, the unbalanced gradients will recover the system of the metabolite of interest, while the other systems will stay in SQ states and experience a spin echo with unbalanced gradients. This leads to a dephasing of the signal that does not contribute to the total signal. A problem of this approach is that only the signal in a DQ state is preserved while the signal that was in the ZQ state is lost, leading to a loss of 50% of the observable lactate signal. In addition, the use of large crusher gradients that dephase the lipid signal causes an additional loss of the lactate signal owing to diffusion weighting [47].

Chemical shift evolution is different under a DQ or ZQ state. Switching between quantum states leads to a difference between the time point of chemical shift refocusing and the time point of J-coupling refocusing, which results in signal loss with a factor of $\cos(\pi \times J \times t1)$ (t1: the multiple quantum evolution period; J: J-coupling evolution time) [48].

Boer et al. presented a refocused DQ filter, which uses three additional 180° refocusing pulses to recover the signal that evolves during the multiple quantum evolution period, therefore refocusing of both the chemical shift and J-coupling evolution (Figure 1) [48].

3
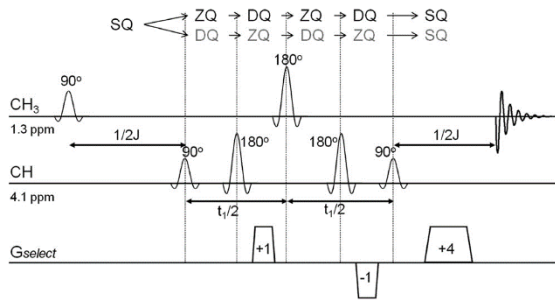
Figure 1. 'Refocused DQ filter sequence for single-shot lactate' by Boer et al [48].

In this study, the use of proton magnetic resonance spectroscopy (1H-MRS) for the measurement of lactate in the portal vein is researched. We explore the feasibility of a refocused DQ filter for lactate measurements in the portal vein. The first results of lactate measurements with a DQF in the presence of flow at 7 Tesla are presented on a flow phantom, in a human brain and in the portal vein.

2 Methods

2.1 Phantom scans

All phantom experiments were performed on a 7 Tesla scanner (Philips, Cleveland, OH), using a 2 transmit, 32 receive channel head coil (Nova Medical, Inc., Burlington, MA). The phantoms were positioned in the center of the coil and the whole setup was placed in the isocenter of the magnet.

Three 50 ml centrifuge tubes were filled with lactate solutions of 2.5 mM, 20 mM and 50 mM in water. The tubes were then placed into a container filled with water for better B0 field homogenization (i.e. B0 shimming) (Figure 2).

Figure 2. Left: 50 ml centrifuge tube filled with a lactate solution. Right: container in which the three centrifuge tubes were placed.

A flow phantom was created, which consisted of a Corio CD-BC4 heating circulator (Julabo, Gmbh., Seelbach, Germany) and a 30 m long tube with an inner diameter of 13 mm. The heating circulator was used to apply a flow up to 924 ml/min. The flow was regulated with a mechanical valve which changes the flow from internal to external (through the tube). The tube was filled with a 3.5 L lactate containing solution (20 mM in water) and was embedded in a water tank for improved B0 shimming (Figure 3).

Figure 3. Water tank with the 13 mm tube looping through the lid of the tank.

STEAM and PRESS sequences were first tested on the phantoms and a STEAM sequence was also tested in a human portal vein. The method used in these tests is described in appendix B.

Hereafter, a refocused double quantum filter (DQF) sequence was implemented in the Philips pulse programming environment (R.5.1.7) on C++ according to Boer et al. and figure 1 [48].

The centrifuge tubes containing different concentrations of lactate solutions were scanned with the DQF sequence (1/2J = 72 ms, t1 = 50 ms, voxel size = 30x30x30 mm^3, number of averages (NSA) = 200, repetition time (TR) = 2000 ms, acquisition bandwidth = 4000 Hz, number of samples = 2048).

Hereafter, the DQF sequence was used to measure the lactate solution stagnant in the 13 mm tube (1/2J = 72 ms, t1 = 50 ms, voxel size = 70x280x280 mm, number of averages (NSA) = 200, repetition time (TR) = 2000 ms, acquisition bandwidth = 4000 Hz, number of samples = 2048). Subsequently, a measurement was performed with a flow of 924 ml/min (1/2J = 72 ms, t1 = 50 ms, voxel size = 30x30x30 mm, number of averages (NSA) = 128, repetition time (TR) = 4000 ms, acquisition bandwidth = 4000 Hz, number of samples = 2048). Lastly, a scan was

performed to examine the lipid suppression capability of the currently implemented sequence. The box filled with water was replaced by a box filled with sunflower oil and a scan with the lactate solution stagnant in the tube was performed (1/2J = 72 ms, t1 = 50 ms, voxel size = 70x280x280 mm, number of averages (NSA) = 200, repetition time (TR) = 2000 ms, acquisition bandwidth = 4000 Hz, number of samples = 2048).

All spectra were visualized with the signal intensity in arbitrary units (AU) on the y-axis and the chemical shift in parts per million (ppm) on the x-axis, using a home-built Matlab (The Mathworks, Inc., Natick, Massachusetts) script for MRS postprocessing.

Only zero order phasing was applied after Fourier transforming to the frequency domain to the spectrum of the centrifuge tubes and the lactate solution stagnant in the flow phantom.

The linewidth of the peaks was determined by calculating the full width at half maximum (FWHM). The SNR of the peak at 1.3 ppm was calculated using Matlab and the equation:

$$SNR = real(\max peak\ height)/abs(std(noise)) \qquad [49]$$

The noise was determined by selecting 25 consecutive peaks in an area in the spectrum without metabolite signal.

As the flow caused artefacts in the entire spectral range, a Hamming apodization filter with a 30 Hz bandwidth was applied to the data obtained in a flow before Fourier transforming to the frequency domain. Hereafter, only zero order phasing was applied.

2.2 In vivo scans

The refocused DQF sequence was also tested on the brain of a volunteer, as studies have shown that it is possible to detect lactate in the brain [29, 30, 35]. Unlocalized (the whole brain) and localized (single voxel positioned in the middle of the brain) scans were performed ($1/2J = 72$ ms, $t1 = 50$ ms, voxel size = 30x30x70 mm, NSA = 32 unlocalized and NSA = 64 localized, TR = 4000 ms, acquisition bandwidth = 4000 Hz, number

of samples = 2048). A 20 Hz Gaussian apodization filter was applied on the data before Fourier transforming to the frequency domain. Hereafter, only zero order phasing was applied.

In order to test the correct functioning of the DQF sequence on the vena porta, lactate concentration needed to be increased in the body. This can be done with an high intensity interval training (HIIT), that has proven to elevate lactate concentrations [50]. Therefore, the DQF sequence was tested on the portal vein of a volunteer after the volunteer had performed a HIIT session. The HIIT session consisted of three 30-second sprints interspersed with 4 minutes of jogging ($1/2J = 72$ ms, $t1 = 50$ ms, voxel size = 30x30x70 mm, NSA = 64, TR = 4000 ms, acquisition bandwidth = 4000 Hz, number of samples = 2048). Only zero order phasing was applied after Fourier transforming to the frequency domain.

3 Results

3.1 Phantom scans

Lactate was detected with the STEAM, PRESS and DQF sequences in the centrifuge tubes containing 2.5, 20 and 50 mM lactate solution. Scanning 20 mM lactate solution stagnant in the flow phantom with the DQF sequence provided a spectrum with a visible lactate peak (Figure 4).

Lactate was also detected in a flow of 924 ml/min. The spectrum obtained in flow showed a lower peak and SNR than the spectrum of the stagnant solution (Figure 5).

The spectrum obtained by scanning the tube in oil showed artifacts in the whole spectral range and no lactate peak was discernable (not shown).
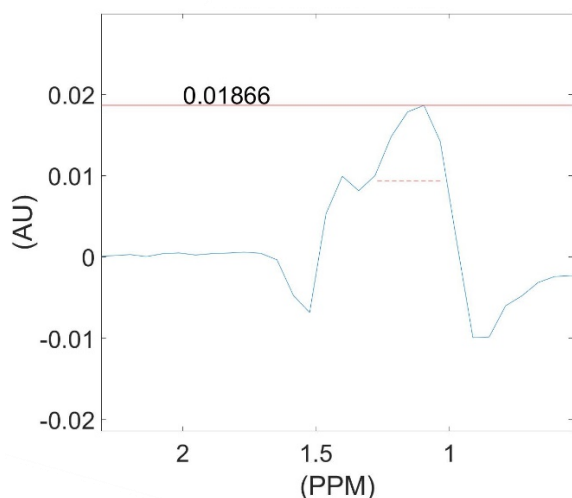
Figure 4. Spectrum of 20 mM lactate solution stagnant in a 13 mm tube, scanned with the refocused double quantum filter sequence. Showing the lactate doublet at 1.33 ppm. SNR: 42.7982. FWHM: 72.9 Hz (0.2447 ppm).
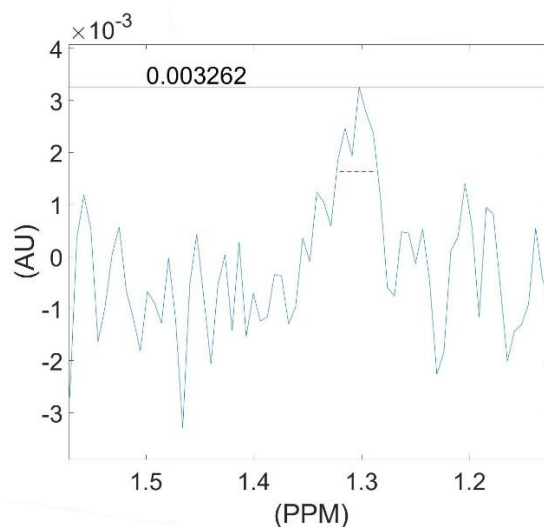
Figure 5. Spectrum of 20 mM lactate solution in a flow of 924 ml/min in a 13 mm tube, scanned with the refocused double quantum filter sequence. SNR: 2.8816. FWHM: 9.8 Hz (0.0328 ppm).

3.2 In vivo scans

The spectrum of the STEAM scan of the blood in the portal vein showed only a large lipid peak at 1.3 ppm.

The spectrum of the unlocalized scan of the brain shows several peaks; at 2.0 ppm, 1.3 ppm, 0.9 ppm and 0.5 ppm (figure 6), which agrees with a lipids spectral profile.

In the spectrum of the localized scan a peak at 1.3 ppm is visible, but with a broad linewidth (107.4 Hz) (figure 7).

The spectrum of the portal vein after a HIIT session shows a large peak at 1.3 ppm (figure 8). However, the presence of the peaks around 2.1 ppm and 0.9 ppm points to a lipid spectrum.
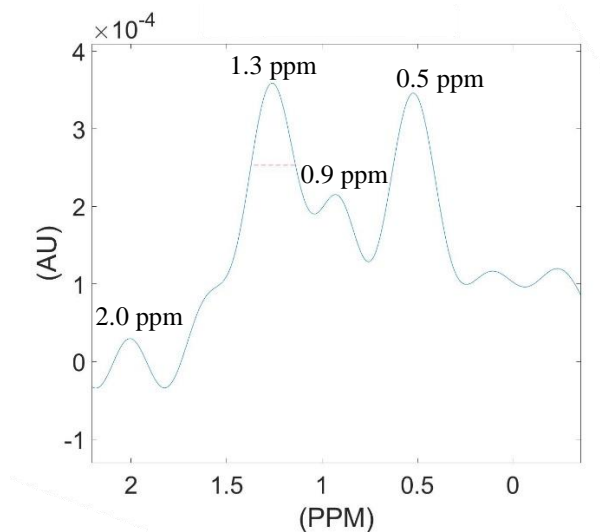
Figure 6. Spectrum of a brain scan with an unlocalized refocused DQF sequence, showing peaks at 2.0 ppm, 1.3 ppm, 0.9 ppm and 0.5 ppm. FWHM: 68.4 Hz (0.2294 ppm).
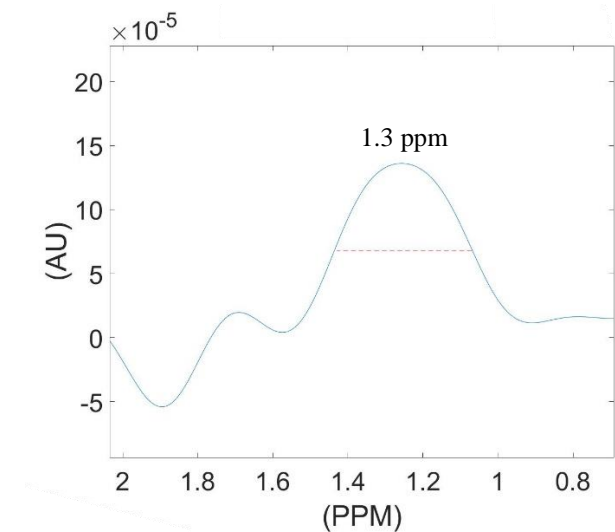
Figure 7. Spectrum of a brain scan with a localized refocused DQF sequence, showing only a peak at 1.3 ppm. FWHM: 107.4 Hz (0.3604 ppm).
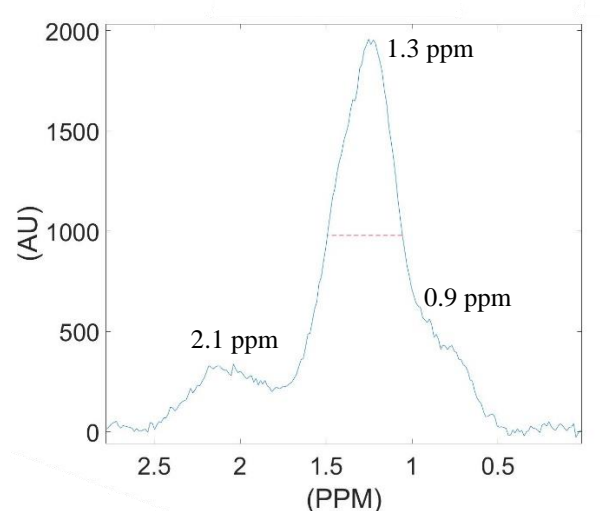
Figure 8. Spectrum of a portal vein scanned withe the DQF sequence after a HIIT session, showing peaks at 2.1 ppm, 1.3 ppm and 0.9 ppm. FWHM: 128.9 Hz (0.4325 ppm).

4   Discussion

The STEAM, PRESS and refocused DQF sequences were successful in detecting lactate in stagnant phantoms of 2.5, 20 and 50 mM. Furthermore, the DQF sequence was successful in detecting 20 mM lactate solution in the presence of a flow of 924 ml/min. Scans measured in the brain and portal vein of healthy volunteers show peaks around 1.3 ppm. However, it is not certain that these peaks are caused solely by lactate. Particularly the spectrum measured from the portal vein showed the presence of a 2.1 ppm, a 0.9 ppm and a 1.3 ppm peak that corresponds to a lipid spectrum [38]. However, despite the presence of flow in the portal vein, narrow bandwidths were obtained that made the individual peak differentiation possible.

It has been shown previously that lactate detection in a flow using 1H-MRS is possible [39]. However, the overlapping lipid signal provides a problem in the measurement of lactate in vivo [37, 38]. The refocused DQ filter presented by Boer et al. can be used to detect lactate whilst dephasing the lipid signal in a calf muscle and the current study has shown that it can be used to detect lactate in a flow [48].

Previous studies have shown that 1H-MRS can be used to detect lactate in the brain [29, 35, 51, 52]. However, the maximum concentration of lactate found in the brain of healthy volunteers was only 1.0 mM [51]. The volunteer of whom the brain was scanned did not have any abdominal symptoms matching AMI or CMI. Therefore, her serological lactate levels while rested would most likely be lower than 2.2 mM. The current study did not determine whether or not lactate concentrations below 2.5 mM could be measured with the DQF sequence. It is possible that no lactate was detected, due to the brain lactate concentration in the volunteer being lower than the detection limit.

The DQF performance in a lipid rich environment showed artifacts in the whole spectral range. Due to the high gradient strengths and the amount of RF pulses used in this sequence in order to suppress the lipid signals, this sequence becomes more sensitive to motion (i.e. flow, breathing, cardiac beating), which makes the detection of lactate in the portal vein with DQF challenging. This also explains why in the presence of flow the signal is below the detection level. More averaging might be a way to circumvent this. However, the motion sensitivity of DQF also explains why it is challenging for the detection of lactate in vivo, given that signal from the moving blood should feel

all DQF RF pulses, which is clearly not the case.

Partial volume and chemical shift displacement (CSDA) artifacts during in vivo measurements of the portal vein were additional sources of lipid contamination in the spectrum. An editing scheme for lactate detection might still be possible for in vivo applications, when including broad banded RF pulses to minimize CSDA and partial volume effects.

The flow in the portal vein makes the detection of lactate much more challenging. Even with large excitation volumes, by the time the last pulse on the DQF sequence is applied, part of the signal has left the volume of interest (VOI) (A quantification simulation of this effect can be found in appendix C). In addition, the movement of the blood and the abdomen due to breathing, leads to additional B0 field artifacts that lead to an increase of the peak's spectral linewidth and to RF frequency offsets, ending in an even lower signal. Therefore, turbulence effects and blood flow within the vessels are detriment for the measurement. Acquisitions with the DQF sequence will benefit from cardiac triggering to acquire at the moment when blood is at its lowest flow or almost still.

Spins that are moving in a flow develop phase variations, which causes a decrease in signal intensity [37]. In MR imaging, rephasing gradients are used to force the phase of the moving spins to be zero at the time of the echo time [53]. Lactate measurement in the portal vein using the refocused DQF sequence may benefit from altering the rephasing gradients so that the phase of the moving spins in the blood flow is zero at the time of the echo.

In summary, 1H-MRS is a promising technique for the diagnosis of acute and chronic mesenteric ischemia. The DQF sequence presented in this study can be used to detect lactate in a flow. However, the sequence cannot measure lactate in the portal vein in the current configuration. Implementation of broad banded RF pulses, cardiac triggering and altering the refocusing gradients to compensate for flow should be investigated.

References

1. Chang, J.B. and T.A. Stein, *Mesenteric ischemia: acute and chronic.* Annals of vascular surgery, 2003. **17**(3): p. 323-328.

2. Rubin, R., D.S. Strayer, and E. Rubin, *Rubin's pathology: clinicopathologic foundations of medicine*. 2008: Lippincott Williams & Wilkins.

3. Sreenarasimhaiah, J., *Chronic mesenteric ischemia.* Best Practice & Research Clinical Gastroenterology, 2005. **19**(2): p. 283-295.

4. McKinsey, J.F. and B.L. Gewertz, *Acute mesenteric ischemia.* Surgical Clinics of North America, 1997. **77**(2): p. 307-318.

5. Kolkman, J., J. Reeders, and R. Geelkerken, *Gastro-intestinale chirurgie en gastro-enterologie. VIII. Gastro-enterologische aspecten van chronische maag-darmischemie.* Nederlands Tijdschrift voor Geneeskunde, 2000. **144**(17): p. 792-796.

6. Kolkman, J.J., et al., *Diagnosis and management of splanchnic ischemia.* World journal of gastroenterology: WJG, 2008. **14**(48): p. 7309.

7. Bradbury, A., et al., *Mesenteric ischaemia: a multidisciplinary approach.* British Journal of Surgery, 1995. **82**(11): p. 1446-1459.

8. Stanton, P.E., et al., *Chronic intestinal ischemia: diagnosis and therapy.* Journal of vascular surgery, 1986. **4**(4): p. 338-344.

9. Mensink, P., et al., *Clinical significance of splanchnic artery stenosis.* British Journal of Surgery: Incorporating European Journal of Surgery and Swiss Surgery, 2006. **93**(11): p. 1377-1382.

10. Florim, S., et al., *Acute mesenteric ischaemia: a pictorial review.* Insights into imaging, 2018. **9**(5): p. 673-682.

11. Rubin, R.S., . D. S.; Rubin, E., *Rubin's pathology: Clinicopathologic foundations of medicine*. Sixth ed. 2012: Philadelphia: Wolters Kluwer Health/Lippincott Williams & Wilkins.

12. Savastano, S., et al., *Multislice CT angiography of the celiac and superior mesenteric arteries: comparison with arteriographic findings.* La Radiologia medica, 2002. **103**(5-6): p. 456-463.

13. Catalini, R., et al., *Color Duplex evaluation of the mesenteric artery.* Journal of ultrasound, 2010. **13**(3): p. 118-122.

14. Meaney, J.F., et al., *Gadolinium-enhanced MR angiography of visceral arteries in patients with suspected chronic mesenteric ischemia.* Journal of Magnetic Resonance Imaging, 1997. **7**(1): p. 171-176.

15. Rosow, D.E., et al., *Imaging of acute mesenteric ischemia using multidetector CT and CT angiography in a porcine model.* Journal of gastrointestinal surgery, 2005. **9**(9): p. 1262-1275.

16. Nicoloff, A.D., et al., *Duplex ultrasonography in evaluation of splanchnic artery stenosis.* Surgical Clinics of North America, 1997. **77**(2): p. 339-355.

17. Kolkman, J.J., J.A. Otte, and A.J. Groeneveld, *Gastrointestinal luminal PCO2 tonometry: an update on physiology, methodology and clinical applications.* British journal of anaesthesia, 2000. **84**(1): p. 74-86.

18. Friedland, S., et al., *Diagnosis of chronic mesenteric ischemia by visible light spectroscopy during endoscopy.* Gastrointestinal endoscopy, 2007. **65**(2): p. 294-300.

19. Mensink, P.B., et al., *Gastric exercise tonometry: the key investigation in patients with suspected celiac artery compression syndrome.* Journal of vascular surgery, 2006. **44**(2): p. 277-281.

20. Otte, J.A., et al., *Clinical impact of gastric exercise tonometry on diagnosis and management of chronic gastrointestinal ischemia.* Clinical Gastroenterology and Hepatology, 2005. **3**(7): p. 660-666.

21. van Wijck, K., et al., *Physiology and pathophysiology of splanchnic hypoperfusion and intestinal injury during exercise: strategies for evaluation and prevention.* American journal of physiology-gastrointestinal and liver physiology, 2012. **303**(2): p. G155-G168.

22. Bland, E. and K.J. Burg, *Fluorescence ratio imaging for oxygen measurement in a tissue engineered construct.* Journal of Histotechnology, 2013. **36**(4): p. 119-127.

23. Mensink, P.B., et al., *Twenty-four hour tonometry in patients suspected of chronic gastrointestinal ischemia.* Digestive diseases and sciences, 2008. **53**(1): p. 133-139.

24. Björck, M., et al., *Editor's choice–management of the diseases of mesenteric arteries and veins: clinical practice guidelines of the European Society of Vascular Surgery (ESVS).* European Journal of Vascular and Endovascular Surgery, 2017. **53**(4): p. 460-510.

25. Evennett, N.J., et al., *Systematic review and pooled estimates for the diagnostic accuracy of serological markers for intestinal ischemia.* World journal of surgery, 2009. **33**(7): p. 1374-1383.

26. Demir, I.E., G.O. Ceyhan, and H. Friess, *Beyond lactate: is there a role for serum lactate measurement in diagnosing acute mesenteric ischemia?* Digestive surgery, 2012. **29**(3): p. 226-235.

27. Tiessen, R.G., et al., *An ultrafiltration catheter for monitoring of venous lactate and glucose around myocardial ischemia.* Biosensors and Bioelectronics, 2001. **16**(3): p. 159-167.

28. Blüml, S., *Magnetic resonance spectroscopy: basics*, in *MR spectroscopy of pediatric brain disorders*. 2013, Springer. p. 11-23.

29. Chi, C.-S., et al., *Lactate peak on brain MRS in children with syndromic mitochondrial diseases.* Journal of the Chinese Medical Association, 2011. **74**(7): p. 305-309.

30. Lunsing, R.J., et al., *Diagnostic value of MRS-quantified brain tissue lactate level in identifying children with mitochondrial disorders.* European radiology, 2017. **27**(3): p. 976-984.

31. Lange, T., et al., *Pitfalls in lactate measurements at 3T.* American journal of neuroradiology, 2006. **27**(4): p. 895-901.

32. Annarao, K.T., et al. *In vivo lactate T1 and T2 relaxation measurements in ER-positive breast tumors using SS1-SelMQC editing sequence.* in *International Society of Magnetic Resonance Medicine*. 2012.

33. Yaligar, J., et al., *Lactate MRSI and DCE MRI as surrogate markers of prostate tumor aggressiveness.* NMR in biomedicine, 2012. **25**(1): p. 113-122.

34. Star-Lack, J., et al., *In VivoLactate Editing with Simultaneous Detection of Choline, Creatine, NAA, and Lipid Singlets at 1.5 T Using PRESS Excitation with Applications to the Study of Brain and Head and Neck Tumors.* Journal of magnetic resonance, 1998. **133**(2): p. 243-254.

35. Choi, C., et al., *Proton spectral editing for discrimination of lactate and threonine 1.31 ppm resonances in human brain in vivo.* Magnetic Resonance in Medicine: An Official Journal of the International Society for Magnetic Resonance in Medicine, 2006. **56**(3): p. 660-665.

36. Andreychenko, A., et al., *Efficient spectral editing at 7 T: GABA detection with MEGA-sLASER.* Magnetic resonance in medicine, 2012. **68**(4): p. 1018-1025.

37. Brix, G., et al., *Basics of magnetic resonance imaging and magnetic resonance spectroscopy*, in *Magnetic Resonance Tomography*. 2008, Springer. p. 3-167.

38. Kuesel, A.C., et al., *1H MRS of high grade astrocytomas: mobile lipid accumulation in necrotic tissue.* NMR in biomedicine, 1994. **7**(3): p. 149-155.

39. Van Leersum, C.M., *Magnetic resonance spectroscopy as a diagnostic tool for chronic splanchnic syndrome.* Technical Medicine Master 3 Internship Report, 2015.

40. Ymker, M., *The measurement of a lactate gap between the liver and the spleen with MR spectroscopy as a marker for gastrointestinal ischemia.* Technical Medicine Master 2 Internship Report, 2009.

41. Mulder, I., Technical Medicine Master 2 Internship Report, 2010.

42. Saris, A., Technical Medicine Master 2 Internship Report, 2011.

43. De Jonge, P., Technical Medicine Master 2 Internship Report, 2011.

44. Zhou, L., *Determination of lactate in portal venous blood flow with use of 3T ¹H-MRS as a diagnostic tool for patients with Chronic Splanchnic Ischemia: a flow phantom experiment.* Technical Medicine Master 2 Internship Report, 2012.

45. De Graaf, R.A., *In vivo NMR spectroscopy: principles and techniques.* 2019: Wiley.

46. Bax, A., et al., *Seperation of the different orders of NMR multiple-quantum transitions by the use of pulsed field gradients.* 1979.

47. He, Q., et al., *Single-scan in vivo lactate editing with complete lipid and water suppression by selective multiple-quantum-coherence transfer (Sel-MQC) with application to tumors.* Journal of Magnetic Resonance, Series B, 1995. **106**(3): p. 203-211.

48. Boer, V.O., P.R. Luijten, and D.W. J. Klomp, *Refocused double-quantum editing for lactate detection at 7 T.* Magnetic resonance in medicine, 2013. **69**(1): p. 1-6.

49. van Oosterom, A. and T.F. Oostendorp, *Medische fysica.* 2011, Amsterdam: Reed Business.

50. Rooijackers, H.M., et al., *A single bout of high-intensity interval training reduces awareness of subsequent hypoglycemia in patients with type 1 diabetes.* Diabetes, 2017: p. db161535.

51. Frahm, J., et al., *Localized proton NMR spectroscopy in different regions of the human brain in vivo. Relaxation times and concentrations of cerebral metabolites.* Magnetic Resonance in Medicine, 1989. **11**(1): p. 47-63.

52. Sappey-Marinier, D., et al., *Proton magnetic resonance spectroscopy of human brain: applications to normal white matter, chronic infarction, and MRI white matter signal hyperintensities.* Magnetic resonance in medicine, 1992. **26**(2): p. 313-327.

53. Haacke, E.M. and G.W. Lenz, *Improving MR image quality in the presence of motion by using rephasing gradients.* American journal of roentgenology, 1987. **148**(6): p. 1251-1258.

54. Giancoli, D.C., *Physics for scientists and engineers*. 2008: Pearson Education International.

55. van Petersen, A.S., et al., *Mesenteric stenosis, collaterals, and compensatory blood flow*. Journal of vascular surgery, 2014. **60**(1): p. 111-119. e2.

56. Moneta, G.L., et al., *Mesenteric duplex scanning: a blinded prospective study*. Journal of vascular surgery, 1993. **17**(1): p. 79-86.

57. Gourdin, M. and P. Dubois, *Impact of ischemia on cellular metabolism*, in *Artery Bypass*. 2013, InTech.

58. Boron, W.F. and E.L. Boulpaep, *Medical physiology : a cellular and molecular approach*. 2009, Philadelphia, PA: Saunders/Elsevier.

59. Benaron, D.A., et al., *Continuous, noninvasive, and localized microvascular tissue oximetry using visible light spectroscopy*. Anesthesiology: The Journal of the American Society of Anesthesiologists, 2004. **100**(6): p. 1469-1475.

60. de Graaf, R.A. and K. Nicolay, *Adiabatic water suppression using frequency selective excitation*. Magnetic resonance in medicine, 1998. **40**(5): p. 690-696.

61. Raaijmakers, A.J., et al., *The fractionated dipole antenna: A new antenna for body imaging at 7 T esla*. Magnetic resonance in medicine, 2016. **75**(3): p. 1366-1374.

Appendix A: Diagnostic techniques for mesenteric ischemia

Imaging

Currently used imaging techniques for diagnosing stenosis or occlusions in the GI blood supply are duplex ultrasound, magnetic resonance angiography (MRA), computed tomography angiography (CTA) and digital subtraction angiography (DSA) [6].

Duplex ultrasound can be used for blood-flow measurements. The blood flow increases around stenotic areas, as it flows through a smaller lumen [54, 55]. However, the ability to measure blood velocity with this technique is dependent on the experience of the operator, due to complex anatomy, movement (breathing), overlying bowel gas, angulation of arteries and difficulty to measure at the precise stenosis position [7, 56].

Images of the supplying vessels and even collateral arteries created with MRA, CTA or DSA are sufficient to evaluate for stenosis [14, 15]. However, they cannot be used to diagnose early mesenteric ischemia directly [16].

Function Tests

Currently, the only clinically available and validated tests for diagnosing mesenteric ischemia are tonometry and visual light spectroscopy (VLS) [17, 19, 20].

Tonometry is used to measure the carbon dioxide tension (pCO_2) in the stomach and jejunum [5, 21]. It relies on the principle that ischemia in tissue leads to accumulation of carbon dioxide, because of the anaerobic production of adenosine triphosphate (ATP) [57, 58]. ATP is an organic chemical that provides energy for several cellular processes. In the absence of oxygen, the process of ATP production is as follows:

$$C_6H_{12}O_6(glucose) + 2\ ADP + 2\ P_i \rightarrow$$
$$2\ C_3H_5O_3^-(lactate) + 2\ ATP + 2\ H^+$$
$$+\ heat$$
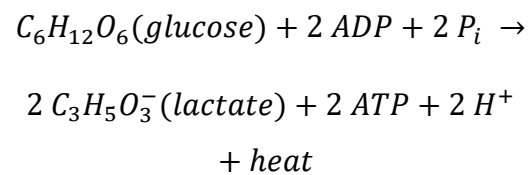
1– 1: ADP = Adenosine diphosphate, P_i = inorganic phosphate, H^+ = hydrogen. [58]

The increase in lactate production causes a decrease in pH level. Carbon dioxide is produced to buffer the decreasing pH which leads to an increased pCO_2 [58].

VLS uses a fiberoptic probe on an endoscope to measure the percent of saturation of hemoglobin in the mucosa of the intestine [18, 59].

Appendix B: STEAM and PRESS tests

Simulations

In order to determine the best scanning parameters for the highest lactate doublet amplitude using a STEAM sequence or a PRESS at 7T, quantum mechanical simulations were made in Bruker's Topspin software (version 4.0.4). This program simulates the behavior of a defined spin system (in this case lactate or lactate + lipids) for the sequence of interest. The shape, power and offset frequency of each pulse on the sequence were changed to test different configurations.

TEs from 1 to 144 ms with steps of 6 ms and TMs from 1 to 70 ms with steps of 5 were tested. Steps of 1 ms from the TEs and TMs that provided the highest lactate signal were also examined. The best spectra were documented.

The first experiments focused on finding the best combination of TE and TM for STEAM and TE for PRESS that provided the highest lactate doublet. As the water concentration in tissue is much higher than most other metabolites, suppression of the water signal is required to visualize other metabolites in the spectrum when scanning the portal vein [60]. Therefore, both sequences started with a 180° rectangular pulse to simulate water suppression.

The highest doublet amplitude for the lactate system found with STEAM was found at TM = 27 ms. At TE = 10 ms the highest doublet with the best absorption phase was found.

PRESS provided the highest lactate doublet at TE = 19 ms.

Phantom tests

The phantom containing the three centrifuge tubes and a flow phantom (flow phantom 2) have already been described in the article. Another flow phantom was constructed (flow phantom 1), which consisted of a water-filled pipe with one end sealed and an open end to which a screw cap could be applied (figure 9). The diameter of the pipe was 9 cm and the length 20 cm. The contrast pump available was used to create constant, known flow in the tube. Tubing of a contrast pump looped through the water-filled pipe, with the endings exiting the pipe through the screw cap. Using the contrast pump, a fluid could be pumped through the tubing with a known flow velocity.

Figure 9. Flow phantom. Left: Screw cap with contrast pump tubing looping through. Right: Water filled pipe, on which the lid can be screwed.

The centrifuge tubes phantom and flow phantom 1 were measured with STEAM, PRESS and the DQF sequence, using the optimal parameters found with TopSpin.

All phantom experiments were performed at a 7 Tesla scanner (Philips, Cleveland, OH), using a 2 transmit, 32 receive channel head coil (Nova Medical, Inc., Burlington, MA). The phantoms were positioned in the center of the coil.

STEAM (TE/TM = 9.4/28, 12/69 and 19/12 ms, TR = 2000 ms, voxel size = 30x30x30 mm, number of signal averages (NSA) = 64 and 240, 2048 samples, acquisition bandwidth = 4000 Hz) and PRESS (TE = 19 ms, TR = 2000 ms, voxel size = 30x30x30 mm, NSA=, 2048

samples, acquisition bandwidth = 4000 Hz) sequences were used. The first sequence parameters were those found from the TopSpin simulations. Several different combinations of settings were tested to find which provided the highest lactate peak with the best SNR.

After scanning the static phantom, tests were performed on flow phantom 1. STEAM (TE/TM = 19/12 ms, TR = 2000 ms, voxel size = 30x30x30, NSA = 240, 2048 samples, acquisition bandwidth = 4000 Hz). 200 ml of 20 mM lactate solution at a flow of 942 ml/min was pumped through the phantom whilst scanning. A scan with the solution stagnant in the phantom was also created to estimate the amount of signal loss and artifacts the flow caused.

The spectra were visualized using a home-built Matlab script for MRS postprocessing and only zero order phasing was applied after Fourier transforming to the frequency domain. The y-axis represents the signal intensity and the x-axis the chemical shift in parts per million (ppm).

In vivo scan

A scan of a human portal vein was performed using a STEAM sequence (TE/TM = 19/12 ms, TR = 4000 ms, voxel size = 30x30x70, NSA = 240, 2048

samples, acquisition bandwidth = 4000 Hz). A body array composed by 8 transceiver fractionated dipole antennas [61], each housing two additional receiver loops was used. The same 7 T whole-body MR system, this time equipped with a parallel transmit system, was used.

The spectrum was visualized using a home-built Matlab script for MRS postprocessing and only zero order phasing was applied after Fourier transforming to the frequency domain.

Appendix C: Quantification of signal loss due to flow

A Matlab (The Mathworks, Inc., Natick, Massachusetts) script was written to simulate the movement of the blood within the MR spectroscopic voxel in the presence of flow, which would give an idea of the signal loss due to flow (Appendix C-1). The script was based on the duration and time stamps of the DQF sequence. The portal vein was simulated as a straight tube with a diameter of 1 cm and a length of 10 cm. This tube was plotted as a graph to visualize where the volume of blood (VOB) that received the first excitation pulse was during the DQF sequence.

A flow and size of the volume of interest (VOI) can be given as input of the script. Based on these settings the script shows where the VOB will be at the time point of each subsequent pulse.

The blood volume receiving the excitation pulse is colored black. For each subsequent pulse the VOB has been given a different color. Next to the simulated portal vein a bar graph is given that shows the overlap of each VOB with the initial scanned volume. The last bar shows the volume that received all pulses and provides the signal.

The results from the portal vein simulations are provided in two graphs. Figures 10 and 11 show the location of the initially excited VOB of 8x1 cm at each pulse-timepoint. When the signal is acquired, approximately 67% of the blood in the VOI received all pulses at a portal vein flow of 676 ml/min.

Figure 11 shows that at a flow velocity of 1052 ml/min, approximately 45% of the blood that provides the signal, has received all pulses.
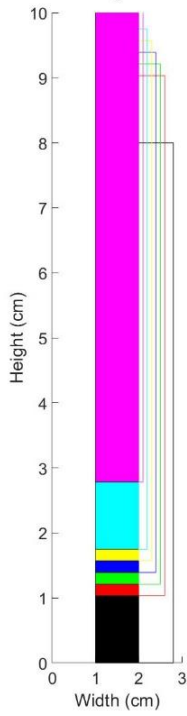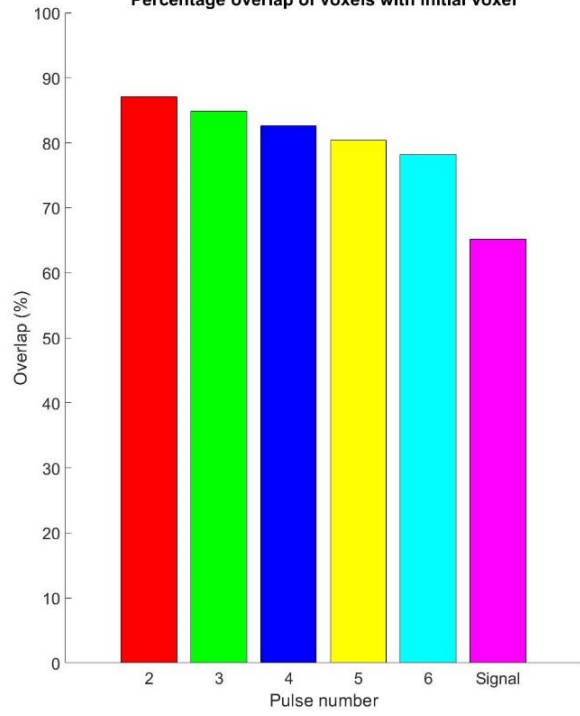
Figure 10. Location and overlap of blood volume during the DQF sequence at the lowest portal vein flow (676 ml/min).
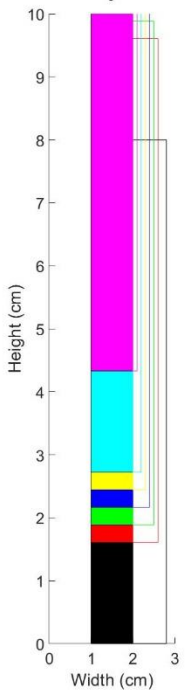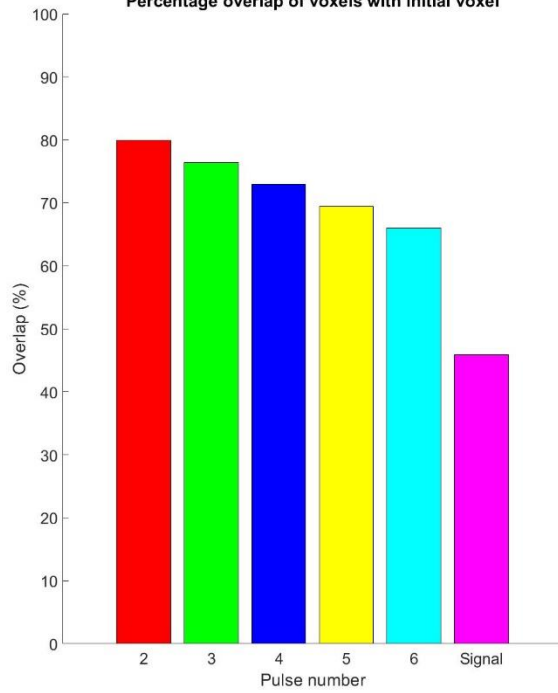
Figure 11. Location and overlap of blood volume during the DQF sequence at the highest portal vein flow (1052 ml/min).

Appendix C-1: Matlab script for portal vein simulation

```matlab
%% Flow cm/s -> ml/min
clear
r = 0.5;                        %Radius in cm
cms = 40;                       %Flow in cm/s
mlm = (pi*(r^2)*cms)*60         %Flow in ml/m


%% Flow ml/min -> cm/s
clear
r = 0.5;                        %Radius in cm
mlm = 676;                      %Flow in ml/min
cms = (mlm/60)/(pi*(r^2))       %Flow in cm/s


%% DQF sequence pulses in order of time: 90, 90, 180, 180, 180, 90.
close all
subplot(1,2,1)
v = 14.3452csi;                 %Blood velocity in cm/s
pp = 72;                        %Preparation period 1/2J in ms
t1 = 50;                        %t1 delay in ms


%width (rw) and height (rh)of voxel
rh = 8;
rw = 1;


%Create portal vein
rectangle('Position',[-1 1 15 1],'EdgeColor',[0 0 0])
hold on
xlim([0 10])
ylim([0 3])
pbaspect([5 1 1]);
xticks(0 : 10)
%set(gca,'YTickLabel',[]);
y = ((1-rw)/2)+1;               %location of voxel on y-axis


%Initial voxel
v1 = rectangle('Position',[0 y rh rw],'FaceColor',[0 0 0]);
pv1 = v1.Position; %Position vector of voxel 1
rectangle('Position',[0 y+rw rh 0.8],'EdgeColor',[0 0 0]);        %Outline on top
of voxel 1 to see its width


% Creating voxels over time
p2 = (v/1000)*pp;
p3 = (v/1000)*(pp+(0.25*t1));
p4 = (v/1000)*(pp+(0.5*t1));
p5 = (v/1000)*(pp+(0.75*t1));
p6 = (v/1000)*(pp+t1);
s =  (v/1000)*(2*pp+t1);


v2 = rectangle('Position',[p2 y rh rw],'FaceColor',[1 0 0]);     %Red voxel at
second 90 degree pulse
v3 = rectangle('Position',[p3 y rh rw],'FaceColor',[0 1 0]);     %Green voxel at
first 180 degree pulse
v4 = rectangle('Position',[p4 y rh rw],'FaceColor',[0 0 1]);     %Dark blue
voxel at second 180 degree pulse
v5 = rectangle('Position',[p5 y rh rw],'FaceColor',[1 1 0]);     %Yellow voxel
at third 180 degree pulse
v6 = rectangle('Position',[p6 y rh rw],'FaceColor',[0 1 1]);     %Light blue
voxel at third 90 degree pulse
v7 = rectangle('Position',[s y rh rw],'FaceColor',[1 0 1]);      %Purple voxel
at signal


rectangle('Position',[p2 y+rw rh 0.6],'EdgeColor',[1 0 0])       %Outline on top
of voxel 2 to see its width
```

```matlab
rectangle('Position',[p3 y+rw rh 0.5],'EdgeColor',[0 1 0])      %Outline on top
of voxel 3 to see its width
rectangle('Position',[p4 y+rw rh 0.4],'EdgeColor',[0 0 1])      %Outline on top
of voxel 4 to see its width
rectangle('Position',[p5 y+rw rh 0.3],'EdgeColor',[1 1 0])      %Outline on top
of voxel 5 to see its width
rectangle('Position',[p6 y+rw rh 0.2],'EdgeColor',[0 1 1])      %Outline on top
of voxel 6 to see its width
rectangle('Position',[s y+rw rh 0.1],'EdgeColor',[1 0 1])      %Outline on top
of voxel 7 to see its width


pv2 = v2.Position;        %Position vector of voxel 2
pv3 = v3.Position;        %Position vector of voxel 3
pv4 = v4.Position;        %Position vector of voxel 4
pv5 = v5.Position;        %Position vector of voxel 5
pv6 = v6.Position;        %Position vector of voxel 6
pv7 = v7.Position;        %Position vector of voxel 7

% Percentages of how much of the initial area is hit
sv1 = pv1(3)*pv1(4);                     %Size of initial voxel
h2 = (rectint(pv1,pv2)/sv1)*100;         %Overlap of voxel 1 and voxel 2
h3 = (rectint(pv1,pv3)/sv1)*100;         %Overlap of voxel 1 and voxel 3
h4 = (rectint(pv1,pv4)/sv1)*100;         %Overlap of voxel 1 and voxel 4
h5 = (rectint(pv1,pv5)/sv1)*100;         %Overlap of voxel 1 and voxel 5
h6 = (rectint(pv1,pv6)/sv1)*100;         %Overlap of voxel 1 and voxel 6
h7 = (rectint(pv1,pv7)/sv1)*100;         %Overlap of voxel 1 and voxel 7
data = [h2 h3 h4 h5 h6 h7];
set(gca,'XAxisLocation','top','YAxisLocation','left','ydir','reverse')
set(gca,'FontSize',20)
camroll(90)
title(['Portal vein with a voxel of ' num2str(rh) ' by ' num2str(rw) ' cm at
different timestamps']);
xlabel('Height (cm)')
ylabel('Width (cm)')

% Create barplot with overlap percentages
cmap = [1 0 0; 0 1 0; 0 0 1; 1 1 0; 0 1 1; 1 0 1];
subplot(1,2,2)
hold on
for i = 1:numel(data)
    bar(i, data(i), 'facecolor', cmap(i,:));
end
set(gca, 'XTick', 1:6, 'XTickLabel', {'2', '3', '4', '5', '6', 'Signal'})
set(gca,'FontSize',20)
ylim([0 100])
title('Percentage overlap of voxels with initial voxel');
xlabel('Pulse number')
ylabel('Overlap (%)')
table(h2,h3,h4,h5,h6,h7)
```